ACS Catalysis

Open Access
This article is licensed under CC-BY 4.0

pubs.acs.org/acscatalysis
Research Article

Factors Affecting the Generation and Catalytic Activity of Extra-Framework Aluminum Lewis Acid Sites in Aluminum-Exchanged Zeolites

Syeda R. Batool, Vitaly L. Sushkevich, and Jeroen A. van Bokhoven*

Cite This: ACS Catal. 2024, 14, 678−690
Read Online

ACCESS | Metrics & More | Article Recommendations | Supporting Information

ABSTRACT: Aluminum ion exchange was employed to introduce Lewis acidity into zeolites BEA, mordenite (MOR), MFI, and FAU (Si/Al = 11−15) and thereby evaluate what factors affect the generation and activity of extra-framework Lewis acid sites (LAS) in zeolites. After the treatment, all zeolites retain their framework structure and porosity characteristics, as evidenced by diffraction and nitrogen physisorption. The increase in the total aluminum content in BEA and FAU was appreciable, whereas MOR and MFI showed very little uptake of aluminum. The increase in total aluminum content quantitatively follows the increase in total LAS content determined by Fourier transform infrared (FTIR) spectroscopy of adsorbed pyridine after dehydration and increases the concentration of octahedrally coordinated extra-framework aluminum after hydration, determined by ^{27}Al magic-angle spinning (MAS) and multiple-quantum magic-angle spinning (MQMAS) NMR spectroscopy. Likewise, the catalytic activity for Meerwein−Ponndorf−Verley reduction of 4-*tert*-butylcyclohexanone changed accordingly with no significant change in MOR and MFI and significant and maximum increase in BEA and FAU. The selectivity of zeolites toward *cis* respectively *trans* 4-*tert*-butylcyclohexanols was affected by the pore size and framework type of the zeolite and not by the number or structure (extra-framework/framework-associated aluminum) of LAS they contain. While the number of LAS in BEA and FAU significantly increased, their total Brønsted acid site (BAS) content remained constant, suggesting that the incorporated LAS are neutral moieties. The incorporation of extra-framework LAS by aluminum ion exchange and their catalytic activity depend on the zeolite framework type, pore size, and possibly on the aluminum location within the zeolite framework.

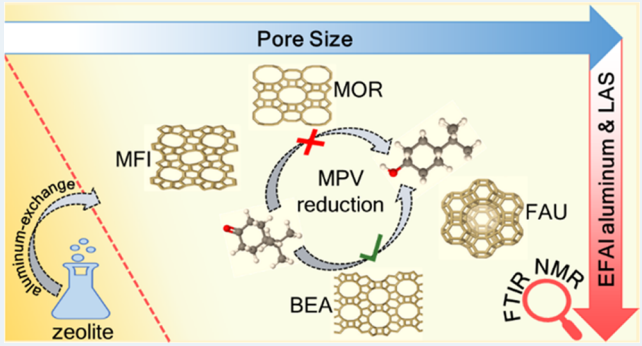

KEYWORDS: *extra-framework EF cations, zeolites, heterogeneous catalysis, Lewis acidity, pyridine, FTIR spectroscopy, NMR spectroscopy, MPV reduction*

Downloaded via LIB4RI on January 5, 2024 at 08:13:22 (UTC).
See https://pubs.acs.org/sharingguidelines for options on how to legitimately share published articles.

1. INTRODUCTION

Zeolites, as an imperative class of heterogeneous catalysts, have found a broad range of applications in many industrially relevant catalytic processes, such as alkylation,[1] isomerization,[2] cracking,[3] and biomass valorization reactions.[4−6] The catalytic activity of these aluminosilicate materials stems from two types of acid sites, Brønsted and Lewis acid types. The acidic nature of these acid sites is extensively analyzed by employing Fourier transform infrared spectroscopy (FTIR) of adsorbed bases, enabling the differentiation between Brønsted acid sites (BAS) and Lewis acid sites (LAS).[7,8] Likewise, solid-state ^{27}Al NMR spectroscopy, coupled with multiple quantum NMR technique, quantifies the aluminum coordination.[9−11] The hydroxyl groups (Si−OH−Al) bridging neighboring tetrahedrally coordinated silicon and aluminum in the zeolite framework are the BAS.[12] However, unlike BAS, the structure of aluminum species responsible for the Lewis acidity of zeolites remains nonconclusive, owing to their plural nature and origin.[13,14] Therefore, evaluating the structure and origin of the Lewis acid in zeolites remains an area of active research and discussion. Based on the proposals brought forward regarding the generation and structure of Lewis acidic aluminum in zeolites, they can be classified as framework aluminum (FAl),[15,16] framework-associated aluminum (FA-Al),[14,17] and extra-framework aluminum (EFAl).[18,19]

Postsynthetic treatments, such as high-temperature calcination, acid−base leaching, and steaming,[20] are the most common ways to generate EFAl and FA-Al species with Lewis acidic character. The EFAl can exist in zeolites in different forms, i.e., Al^{3+}, $Al\text{-}(OH)^{2+}$, $Al(OH)^{2+}$, AlOOH,

Received: September 5, 2023
Revised: December 11, 2023
Accepted: December 15, 2023

ACS Publications
© XXXX The Authors. Published by American Chemical Society

https://doi.org/10.1021/acscatal.3c04195
ACS Catal. 2024, 14, 678−690

Table 1. Selected Zeolite Structures with Characteristic Features of their Respective Frameworks[a]

	BEA (Beta)	MOR (Mordenite)	MFI (ZSM5)	FAU (Faujasite Y)
	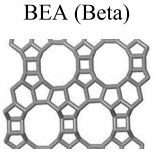	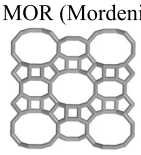	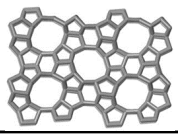	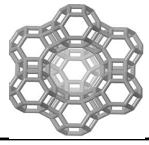
Pore Size (Å)	6.7	6.5	5.3	7.4
Cage diameter (Å)	12.5	-	7.8	12.8
Pore dimensions	3	2	3	3

[a]Data obtained from the database of zeolite structures, structure commission of the International Zeolite Association.[44]

$Al(OH)_3$, and Al_2O_3.[21,22] The FA-Al is an aluminum that is at least partially dislodged from the framework and adapts an octahedral environment under hydrated ^{27}Al NMR conditions, whereas on being ion-exchanged with ammonium, it can reversibly be inserted back into the framework exhibiting tetrahedral coordination. Therefore, FA-Al can easily be distinguished from EFAl, with the former having reversible octahedral−tetrahedral coordination and the latter not reverting into a framework tetrahedral position, mostly adapting an irreversible octahedral environment.[23−26] Likewise, the aluminum in the zeolite framework (FAl) is also reported to act as a Lewis acid site after making extra coordination with a base-like pyridine.[16] The possible origin of framework LAS can be distorted/perturbed framework aluminum or defects in the framework, including those created by dehydroxylation of bridging hydroxyl groups.[27,28] There are a number of challenges associated with the conventional methods used to generate LAS, which particularly include the generation of LAS at the expense of BAS, the generation of multiple LAS structures, and limited control over the fate of LAS.[20−22] A complication in establishing the relation between the structure and performance of aluminum LAS originates from the effectiveness of any postsynthetic modifications being different for zeolites of different structure types.[13,14,29] Furthermore, the literature overlooks the types of aluminum structures that can serve as LAS, and systematic experiments to distinguish EFAl LAS from FA-Al LAS are not usually employed while explaining the Lewis acidity of aluminum zeolites.[14,20]

LAS in zeolites are extensively explored for biomass valorization reactions, such as hydride transfer reactions,[30] conversion of cellulose to glucose,[31] glucose to fructose,[32] trioses to alkyl lactates, and Baeyer−Villiger (BV) oxidation of ketones and aromatic aldehydes.[33,34] LAS are most extensively evaluated in the Meerwein−Ponndorf−Verley reduction of aldehydes and ketones and Oppenauer oxidation of alcohols (MPVO reactions). In the MPVO mechanism, the reaction is initiated by the coordination of the reducing alcohol on a Lewis acidic aluminum center to form an aluminum alkoxide species. This is followed by the coordination of the ketone, resulting in a six-membered ring transition state, to undergo hydride ion transfer from the alkoxide to the carbonyl group of the ketone.[35] The widespread use of these reactions to explore Lewis acidic zeolites is due to the following reasons: (i) these reactions are highly selective to carbonyl groups, and (ii) LAS provides the precursor to form the active site for the hydride transfer mechanism.[36] In our previous work, we introduced the Lewis acidity into zeolite Y by a facile aluminum exchange (Al-IE) method.[37,38] Combining the catalytic tests in the MPV reaction with FTIR and NMR spectroscopies, we quantitatively correlated the Lewis acidity to the EFAl species introduced by Al-IE. Herein, we explore the factors that affect the incorporation of aluminum-exchanged LAS in zeolites of different framework types and their associated catalytic performance.

Employing the MPV reaction as a model LAS-catalyzed reaction can also provide insight into the pore size effect based on the catalytic conversion on zeolite catalysts and selectivity toward *cis*/*trans*-alcohol products.[35,36] Consequently, our objective is to systematically study the generation of aluminum-exchanged EF LAS in different zeolites of similar Si/Al ratios and highlight which parameters play a decisive role while tuning the number of LAS of different zeolites by Al-IE. Thus, we chose zeolite types Y, β, ZSM5, and mordenite for aluminum exchange treatments because (1) these are among the most applied and most investigated zeolite types, (2) these frameworks enable to generate/modulate the LAS in them and explore the factors, such as pore size and Si/Al ratio, that generate LAS, and (3) these zeolites have already been extensively studied in MPV reactions to get deeper insights into the activity, stereoselectivity, active sites, and reaction mechanism.[39−43] We studied these zeolites by pyridine-probed FTIR, ^{27}Al MAS NMR, and catalytic testing in the Meerwein−Ponndorf−Verley (MPV) reduction of 4-*tert*-butylcyclohexanone. Zeolite β (BEA), Y (FAU), and ZSM5 (MFI) have three-dimensional, whereas mordenite (MOR) has semi two-dimensional frameworks (Table 1). Likewise, the pore size in these zeolite topologies is in the following order: zeolite Y > zeolite β > zeolite mordenite > zeolite ZSM5.

This work focuses on the rational design of Lewis acidity in order to counter the challenges posed by conventional methods. We demonstrate that Al-IE is an effective way to enhance the LAS of a zeolite in a controlled way by generating neutral aluminum oxide/hydroxide clusters without affecting the intrinsic structure and Brønsted acidity of the zeolite. The incorporation and activity of EF LAS depend on the type of zeolite, pore size, distribution of aluminum species in the zeolite framework, and the aluminum precursor used to access them. This study can thus provide guidelines for the selection of zeolites for tuning the Lewis acidity by Al-IE and generating Lewis acid catalytic activity into zeolites. Furthermore, this work presents a quantitative differentiation of EFAl LAS from FA-Al LAS with respect to structure, acidity, and activity, obtained through systematic experiments, which is a valuable

https://doi.org/10.1021/acscatal.3c04195
ACS Catal. 2024, 14, 678−690

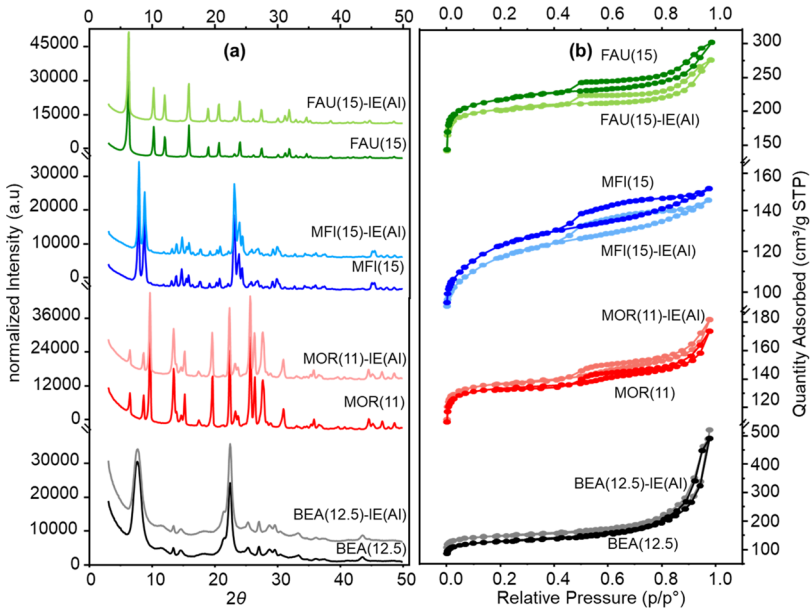

Figure 1. Powder X-ray diffraction (PXRD) patterns (a) and nitrogen adsorption isotherms (b) of the parent zeolite and aluminum-exchanged samples.

development toward the fundamental understanding of the nature of Lewis acidic aluminum in zeolites.

2. RESULTS

The parent proton forms of the zeolites used in this work are labeled as BEA(12.5), MOR(11), MFI(15), and FAU(15). The resultant aluminum-exchanged zeolites are labeled as BEA(12.5)-IE(Al), MOR(11)-IE(Al), MFI(15)-IE(Al), and FAU(15)-IE(Al), respectively. Experimental details on material preparation, characterization, and catalytic testing are given in the Supporting Information (SI) (Sections S1.1−S1.4).

2.1. Physicochemical Characterization. The X-ray diffraction patterns of the parent and aluminum-exchanged zeolites are listed in Figure 1a. The samples BEA(12.5)-IE(Al), MOR(11)-IE(Al), MFI(15)-IE(Al), and FAU(15)-IE(Al) show all the characteristic diffraction peaks, comparable to those in the parent BEA(12.5), MOR(11), MFI(15), and FAU(15), respectively.[14,45] The relative crystallinity[37] of the aluminum-modified zeolites (where the crystallinity of parent zeolites is assumed to be 100%) ranges from 89 to 96%, only indicating a minor change. The comparable intensities of diffraction peaks and relative crystallinity in all samples show that the structure of the zeolites remains preserved after Al-IE treatment. These results rule out the collapse of the zeolite structure due to the development of any amorphous or crystalline impurities such as aluminum oxide agglomerations formed during Al-IE or calcination.

The nitrogen adsorption/desorption isotherms of all samples are presented in Figure 1b, whereas Table 1 summarizes the quantitative characteristics. The parent BEA(12.5) and FAU(15) samples exhibit typical type IV isotherms,[46−48] whereas MFI(15) and MOR (11) show a characteristic type I isotherm.[49] The nitrogen physisorption isotherms of all aluminum-exchanged samples, i.e., BEA(12.5)-IE(Al), MFI(15)-IE(Al), MOR(11)-IE(Al), and FAU(15)-IE(Al), look identical to those of their corresponding parent zeolites. Likewise, the Brunauer−Emmett−Teller (BET) surface areas and micropore volume of zeolites before and after treatment remain almost unchanged, staying within the error limits (Table 1). Thus, not only is the crystallinity virtually unchanged by ion exchange, but the intrinsic porosity and adsorption behavior are not affected.

To compare the varying degrees of aluminum incorporation in different zeolites due to the Al-IE treatment, the bulk Si/Al ratios of zeolites before and after Al-IE, determined by inductively coupled plasma (ICP), are presented in Table 1. The Si/Al ratio values determined for BEA(12.5), MFI(15), MOR(11), and FAU(15) are 12.5, 15, 11, and 15 respectively. The Si/Al ratios for MOR(11)-IE(Al) and MFI(15)-IE(Al) are 10.6 and 13.9, showing only a small decrease as compared with those of parent zeolites. However, in the case of BEA(12.5)-IE(Al) and FAU(15)-IE(Al), the Si/Al ratios of 10.4 and 9.1, respectively, are substantially lower than those of their parent zeolites, indicating ample uptake of aluminum species by these zeolites during Al-IE treatment. Hence, the increase in total aluminum content after Al-IE with respect to the parent zeolites decreases in the following order: FAU(15)-IE(Al) > BEA(12.5)-IE(Al) > MFI(15)-IE(Al) > MOR(11)-IE(Al).

Figures 2 and 3 present the ^{27}Al MAS and ^{27}Al multiple-quantum magic-angle spinning (MQMAS) NMR spectra of the zeolites recorded under ambient conditions, respectively. The F1 axis in MQMAS NMR spectra is an isotropic dimension, whereas the F2 axis presents an anisotropic dimension with second-order quadrupolar interactions (Table 2).

Figure 2 shows the sharp resonances at 54, 57, 57, and 61 ppm in the spectra of BEA(12.5), MOR(11), MFI(25), and FAU(15), respectively, corresponding to tetrahedral aluminum species (Al(IV$_a$)) in the framework of zeolite.[20,50] The ^{27}Al MQMAS NMR spectra (Figure 3a−d) reveal the Al(IV$_a$) resonance on the diagonal (where F1 = F2), thus having a very small quadrupolar interaction of Q_{cc} = 1.4−1.9 MHz (Table 3).

The overall broadening and asymmetric shape of the tetrahedral signal in MAS NMR spectra of some parent zeolites are due to the presence of features other than Al(IV$_a$)

https://doi.org/10.1021/acscatal.3c04195
ACS Catal. 2024, 14, 678−690

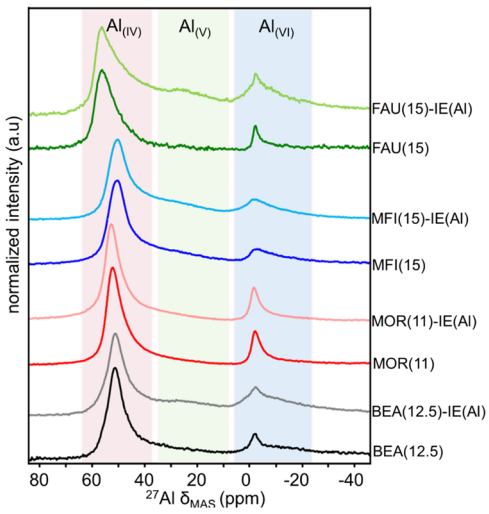

Figure 2. ^{27}Al MAS NMR spectra of parent and aluminum-exchanged zeolites. Colored regions are added to guide the eye.

species. First, a broad resonance, with small Q_{cc} (1.3−1.9 MHz) but slightly greater isotropic broadening, is present at 58.5 and 56.0 ppm in the spectra of BEA(12.5) and FAU(15), respectively, labeled as Al(IV$_b$) species. These Al(IV$_b$) species, in FAU(15), are due to framework aluminum still in tetrahedral coordination but facing a slightly different environment.[37] In the case of zeolite BEA(12.5), however, two types of T sites are present that differ based on their T-O-T angles. Thus, aluminum species on these two T sites are fairly symmetrical yet appear at slightly different chemical shifts in MAS NMR.[47,51] Second, a broad resonance is present in the spectra of BEA(12.5), MOR(11), MFI(15), and FAU(15), at 60.0, 61.5, 62.4, and 63.2 ppm, respectively, that exhibits very large Q_{cc} (3.8−4.5 MHz) and is labeled as Al(IV$_c$) species (Figure 3 and Table 3). These Al(IV$_c$) species are assigned to distorted tetrahedral aluminum, whose fraction varies as a function of calcination temperature, as discussed by Ravi et al.[14] The spectra of BEA(12.5) and FAU(15) also show a small peak in the region 30−35 ppm due to penta-coordinated aluminum species,[52−54] labeled as Al(V) species.

Octahedral aluminum, in the proton form of zeolites, can be characterized as (at least) two different types of species. The aluminum species that can be reinserted back into the framework of the zeolite after ammonium ion exchange (disappearance of resonance in the octahedral region and increase of intensity in the tetrahedral one) are framework-associated aluminum (FA-Al). Those retaining their octahedral coordination in proton and NH_4^+ forms of the zeolite are assigned to EFAl.[14,20,37] The spectra of parent zeolites show a sharp resonance in the octahedral region at 0.1 and 1 ppm (Figure 2). The spectra of the NH_4^+ form of parent zeolites (Figure S1) do not show any peak at 0.1 and 1 ppm, with a corresponding increasing intensity in the tetrahedral region. Thus, these octahedral aluminum, corresponding to the 0.1−1 ppm resonance in proton form of zeolites, which appear as the framework tetrahedral species in NH_4^+ form of these zeolites, are FA-Al (denoted as Al(VI$_a$)).[23] This resonance is narrow in the spectra of BEA(12.5), MOR(11), and FAU(15) samples (Q_{cc} = 1.1−1.4 MHz), whereas, in the spectrum of MFI(15), this peak experiences isotropic broadening, thus having slightly greater Q_{cc} (1.8 MHz) as compared to other parent zeolites (Table 3 and Figure 3a−d).

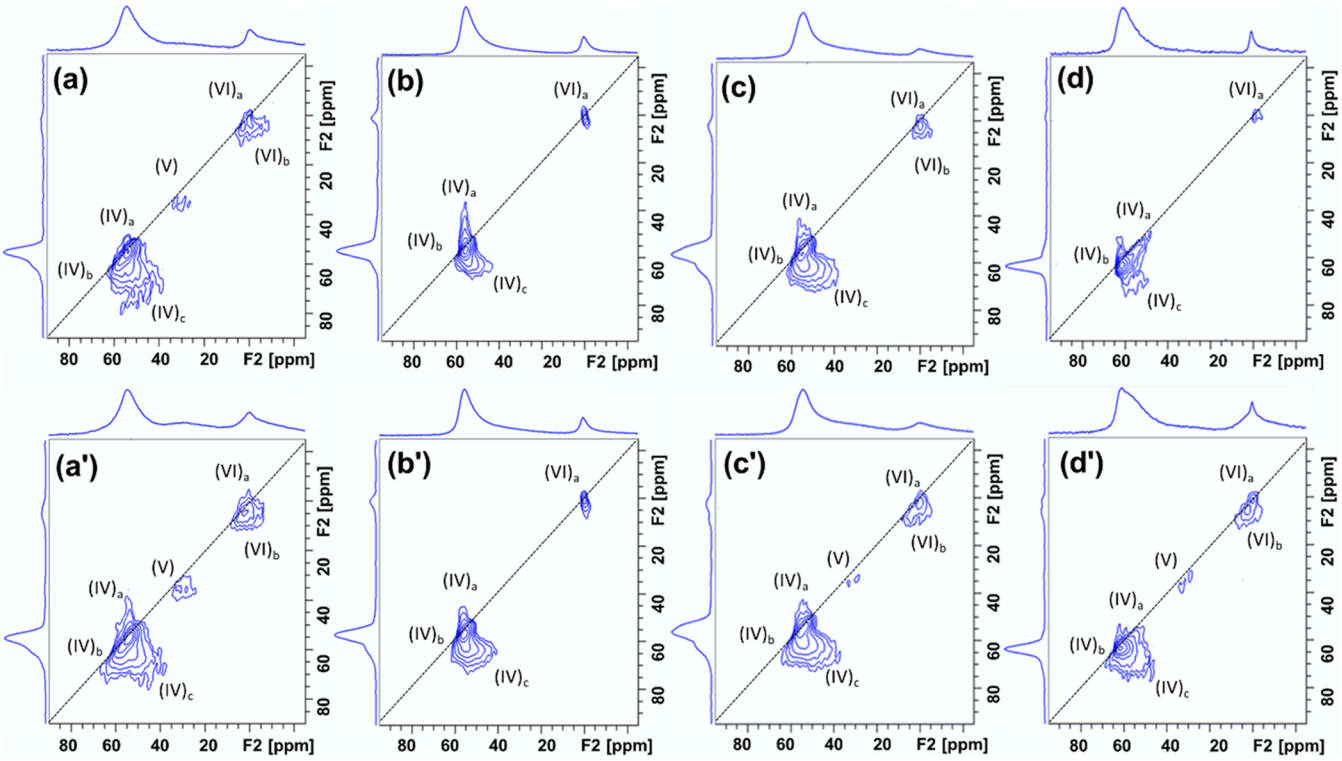

Figure 3. ^{27}Al MQMAS spectra of parent and aluminum-exchanged zeolite BEA (a and a′), MOR (b and b′), MFI (c and c′), and FAU (d and d′) where (a) BEA(12.5), (a′) BEA(12.5)-IE(Al), (b) MOR(11), (b′) MOR(11)-IE(Al), (c) MFI(15), (c′) MFI(15)-IE(Al), (d) FAU(15) and (d′) FAU(15)-IE(Al), respectively.

https://doi.org/10.1021/acscatal.3c04195
ACS Catal. 2024, 14, 678−690

Table 2. Physicochemical Characterization of Parent and Aluminum-Exchanged Zeolites

zeolite	S_{BET} (m^2 g^{-1})[a]	V_{total} (cm^3 g^{-1})[b]	V_{micro} (cm^3 g^{-1})[c]	S_{micro} (m^2 g^{-1})[c]	S_{meso} (m^2 g^{-1})[c]	crystallinity$_{rel}$ (%)[d]	Si/Al ratio[e]
BEA(12.5)	480	0.20	0.20	340	150	100	12.5
BEA(12.5)-IE(Al)	450	0.24	0.21	320	130	89	10.4
MOR(11)	390	0.28	0.18	350	40	100	11.0
MOR(11)-IE(Al)	400	0.29	0.19	360	50	95	10.6
MFI(15)	310	0.14	0.15	280	30	100	15.0
MFI(15)-IE(Al)	310	0.15	0.14	270	40	96	13.9
FAU(15)	700	0.39	0.32	610	190	100	15.0
FAU(15)-IE(Al)	680	0.36	0.3	610	180	90	9.1

[a]Calculated from the BET method. [b]Based on single-point adsorption at p/p_o = 0.97. [c]Calculated from the *t*-plot method. [d]Calculated by a previously described method,[37] assuming the crystallinity of parent zeolites as 100%. [e]Calculated from ICP.

Table 3. NMR Parameters, Including Isotropic Chemical Shift in ppm (δ_{iso}, ± 0.5) and Quadrupolar Coupling Constant in MHz (C_Q, ± 0.3) Obtained from Deconvolution ^{27}Al MQMAS NMR Spectra Using the Czjzek Line Shape Model[55]

		$Al_{(IV)_a}$	$Al_{(IV)_b}$	$Al_{(IV)_c}$	$Al_{(V)}$	$Al_{(VI)_a}$	$Al_{(VI)_b}$
BEA(12.5)	δ_{iso}	54	58.5	60	30	0.1	2.7
	C_Q	1.7	1.9	4.5	2.5	1.1	2.5
MOR(11)	δ_{iso}	57		61.5		0.5	
	C_Q	1.7		3.1		1.4	
MFI(15)	δ_{iso}	56.8		62.4	32	0.9	2.8
	C_Q	1.9		4.2	2.3	2.8	2.4
FAU(15)	δ_{iso}	61	56	63.2	35	1.0	2.9
	C_Q	1.4	1.3	3.8	1.7	1.2	2.8

The spectra of BEA(12.5) and MFI(15) also show an additional broad asymmetric resonance at ∼2.8 ppm, whose intensity does not change in the spectra of the respective NH_4^+ forms (Figure S1). This resonance, irreversible upon NH_4^+ exchange, has significantly large Q_{cc} ∼ 2.7 MHz and a relatively narrow isotropic broadening (Table 3 and Figure 3a,3c). This broad asymmetric resonance at ∼2.8 ppm, labeled Al(VIb), can correlate to EFAl species.

After Al-IE, no significant changes appear in the intensity of any resonances in the spectrum of MOR(11)-IE(Al). However, the intensity of resonance due to EFAl species increases in the spectrum of BEA(12.5)-IE(Al), thus making the feature due to FA-Al species less prominent (Figures 2 and 3a′). Surprisingly, a broad resonance with significant intensity also appears at ∼3 ppm in the spectrum of FAU(15)-IE(Al), which is similar in shape and quadropolar interaction (Q_{cc} = 2.8 MHz) to EFAl species of the BEA(12.5) and BEA(12.5)-IE(Al) (Figure 3 and Table 3). The absence of this resonance in parent FAU(15) shows that the Al-IE in FAU(15)-IE(Al) results in the generation of EFAl species.

In the case of MFI(15)-IE(Al), only a slight intensity increase in the octahedral region is visible, primarily due to FA-Al species (Figures 2 and 3c′). For BEA(12.5)-IE(Al), MFI(15)-IE(Al), and FAU(125)-IE(Al), the intensity of the peak due to the Al(V) species also slightly increases. Lastly, as evident from MQMAS spectra, all aluminum-exchanged samples undergo a slight increase in the intensity of $Al(IV_c)$ species.

Table S1 lists the quantitative analysis of the concentration of aluminum species in different coordinations obtained from MAS NMR spectra using the NMR fitting parameters determined from the MQMAS spectra. This quantitative

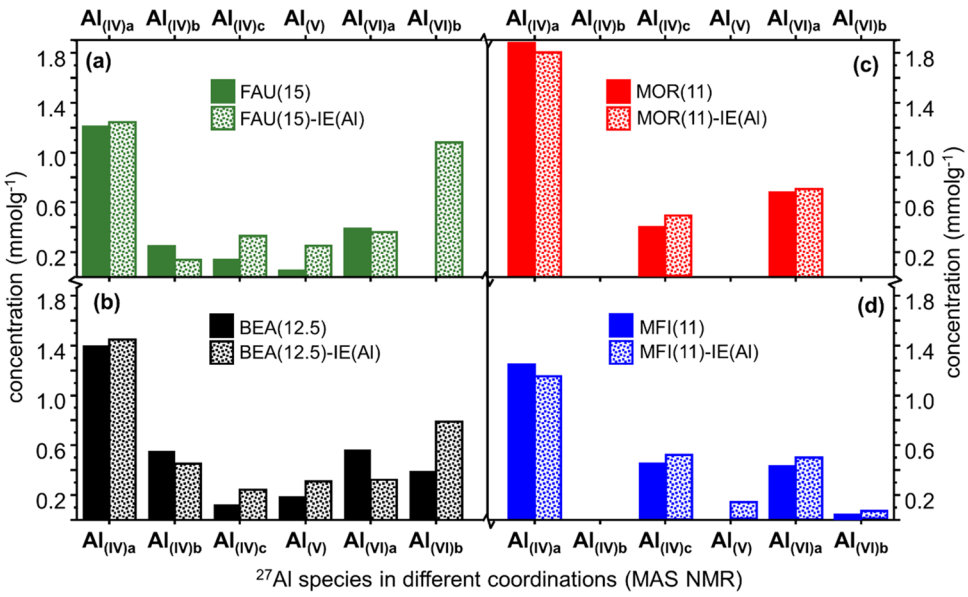

Figure 4. Quantitative distribution (in mmoles g^{-1}, ±10%) of aluminum species, i.e., $Al(IV_a)$, $Al(IV_b)$, $Al(IV_c)$, Al(V), $Al(VI_a)$, $Al(IV_b)$ species obtained from ^{27}Al MAS and MQMAS NMR spectra of parent (solid bars) and aluminum-exchanged (dotted bars) samples of FAU (a), BEA (b), MOR (c), and ZSM5 (d) zeolites.

https://doi.org/10.1021/acscatal.3c04195
ACS Catal. 2024, 14, 678−690

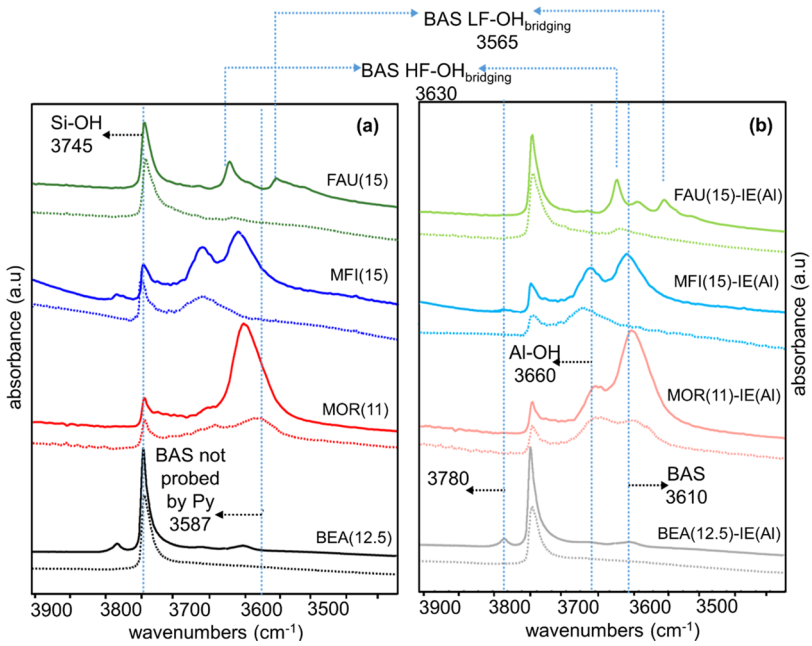

Figure 5. FTIR spectra in hydroxyl stretching region of parent (a) and aluminum-exchanged zeolites (b); solid lines represent spectra of evacuated samples at 723 K, and dotted lines represent spectra after pyridine adsorption at 423 K followed by evacuation at 423 K.

distribution of aluminum species is presented in Figure 4a−d for a clear visual comparison. The quantitative information on the distribution of aluminum species is (with minor discrepancies) in line with the qualitative observations discussed above. After Al-IE, the concentration of Al(IV_c) species is slightly increased in all aluminum-treated samples, followed by a similar decrease in the concentration of Al(IV_a) species in MOR(11)-IE(Al) and MFI(15)-IE(Al) and Al(IV_b) species in FAU(15)-IE(Al) and BEA(12.5)-IE(Al), respectively (Figure 4a−d). The most prominent effect of Al-IE on the aluminum distribution can be observed in zeolites FAU and BEA. The concentration of Al(VIb) species (EFAl) in BEA(12.5)-IE(Al) increases from 0.39 to 0.79 mmol g^{-1} after Al-IE, whereas that of the Al(VI_a) species (FA-Al) slightly decreases from 0.56 to 0.34 mmol g^{-1}. In the case of FAU(15)-IE(Al), Al-IE incorporates 1.08 mmol g^{-1} of the EFAl Al(VI_a) species, while the content of Al(VI_a) species remains comparable to that of FAU(15). There is also a small (but similar) increase in the concentrations of both Al(VI_a) and Al(VIb) in MFI(15)-IE(Al). The increase in the octahedral aluminum content is also followed by a slight increase in Al(V) species content in aluminum-exchanged BEA, FAU, and MFI samples. From these results, the collective concentration of EFAl, after Al-IE, increases in the following order: MOR(11)-IE(Al) < MFI(11)-IE(Al) < FAU(15)-IE(Al) < BEA(12.5)-IE(Al), whereas the EFAl content incorporated after Al-IE increases as follows: MOR(11)-IE(Al) < MFI(11)-IE(Al) ≪ BEA(12.5)-IE(Al) < FAU(15)-IE(Al).

The total aluminum content in zeolites plays an important role that enables zeolites to stabilize different structures of different coordinations within the pores. Therefore, it is necessary to rule out respectively accept the possibility that any change in the Si/Al ratio of MOR and MFI zeolites would affect the incorporation of EFAl species after Al-IE. Therefore, the ^{27}Al MAS NMR of MFI(40) and MOR(45) (with relatively high Si/Al ratios) and their respective aluminum-exchanged samples were recorded (Figure S2b). However, Al-IE, yet again, fails to incorporate any EFAl species in the MFI(40)-IE(Al) and MOR(45)-IE(Al) samples. Only a slight increase in FA-Al species was visible for the MOR(45)-IE(Al) sample (Figure S2b).

2.2. FTIR Spectroscopy and Quantification of Lewis Acidity. The FTIR spectra in the hydroxyl stretching region of parent and aluminum-exchanged zeolites, recorded before (solid spectra) and after pyridine adsorption (dotted spectra), are presented in Figure 5a,b. Before pyridine adsorption, a sharp band at ∼3745 cm^{-1} is present in the spectra of all parent zeolites, ascribed to external silanol groups.[56] The shoulder at ∼3736 cm^{-1} corresponds to internal silanol groups. The band at 3610 cm^{-1} in the spectra of BEA(12.5), MOR(11), and MFI(15) corresponds to the bridging Si-(OH)Al groups (BAS). The spectrum of FAU(15) shows two bands at 3630 and 3565 cm^{-1}, corresponding to high and low-frequency bridging OH groups in super/sodalite cages Figure 5a.

A relatively broad band at ∼3660 cm^{-1} in the spectra of BEA(12.5), MOR(11), and MFI(15) corresponds to framework Al−OH species.[14,57−59] The spectrum of FAU(15) shows two bands at ∼3660 and ∼3597 cm^{-1} due to Al−OH species in the super cage and sodalite cage of zeolite, respectively.[60,61] A band at ∼3780 cm^{-1} in the spectra of BEA(12.5) and MFI(15) is previously assigned to extra-lattice aluminum species, agglomerated in the form of Al_2O_3 microparticles in ZSM5,[62] EFAl in appearing in the octahedral environment in ^{27}Al NMR of BEA zeolite[63] or tricoordinated aluminum connected to the BEA framework.[64] However, the exact assignment of this band still needs to be clarified.

After pyridine adsorption, the intensity of the 3745 cm^{-1} band slightly decreases in the spectra of FAU(15) and MOR(11). The bands at 3780 and 3610 cm^{-1} disappear entirely in the spectra of BEA(12.5) and MFI(15), whereas the latter band decreases in intensity in MOR(11). The low-frequency OH band of FAU (15) also disappears, and the intensity of the high-frequency bridging OH band strongly

https://doi.org/10.1021/acscatal.3c04195
ACS Catal. 2024, 14, 678−690

decreases (Figure 5a). The remaining intensity of BAS bands in MOR(11) and FAU(15) indicates that some of the BAS in these samples is not probed by pyridine due to accessibility hindered by the zeolite pores. Furthermore, the hydroxyl bands due to Al−OH species undergo complete disappearance in BEA(12.5) and (FAU(15) and a minimal decrease in the intensity for MFI(15). No significant difference appears in the Al−OH band of MOR(11).

After aluminum incorporation, the FTIR spectra (before and after pyridine adsorption) of BEA(12.5)-IE(Al) and MFI(15)-1IE(Al) do not reveal any substantial differences in the position or intensity of bands compared to the parent zeolites (Figure 5b). However, the intensity of the bands due to Al−OH species, in the case of MOR(11)-IE(Al) and FAU(15)-IE(Al), increases in intensity (at 3660 and 3597 cm^{-1}, respectively). The intensity of the 3660 cm^{-1} band in MOR has been established to be directly proportional to the amount of highly distorted tetrahedral aluminum.[14] We also correlate this band to $Al(VI_a)$ species, as in our experiments, Al-IE treatment was always followed by calcination at temperatures similar to those utilized in ref 14.

Figure 6 presents the FTIR difference spectra of samples, before and after Al-IE, in the pyridine aromatic ring deformation region. The spectra of all samples exhibit five distinct bands at 1455, 1490, 1545, 1621, and 1634 cm^{-1}. The bands at 1455 and 1621 cm^{-1} correspond to aromatic ring deformation vibrations of pyridine bound to LAS, and the bands at 1545 and 1634 cm^{-1} correspond to vibrations of pyridine interacting with BAS.[8,65] The 1490 cm^{-1} band, however, is structure insensitive. The bands at 1445 and 1545 cm^{-1} are utilized to quantify LAS and BAS, respectively[66] (Table 4). The number of resonances in the pyridine stretching region in the spectra of parent zeolites and the respective positions of these bands agree well with those in the literature.[67−72] However, the relative intensities of LAS and BAS might vary in different samples, corresponding to the difference in the synthesis conditions and postsynthetic treatments. Even the different batches of zeolite from the same commercial supplier would have different proportions of LAS and BAS.[67−72] Before Al-IE, the spectrum of BEA(12.5) has the maximum intensity of LAS bands, whereas the spectra of MOR(11), MFI(15), and FAU(15) have similar intensities (but lower than those of BEA(12.5)) of these LAS bands (Figure 6). The intensity of bands due to BAS is the maximum in the spectrum of MOR(11), which, together with a maximum intensity of 3610 cm^{-1} (Figure 5b), can be explained in terms of the lowest Si/Al ratio of MOR(11) as compared to the other parent zeolites. The BAS bands in the spectra of BEA(12.5), MFI(15), and FAU(15) show intensities comparable to each other but lower than MOR(11).

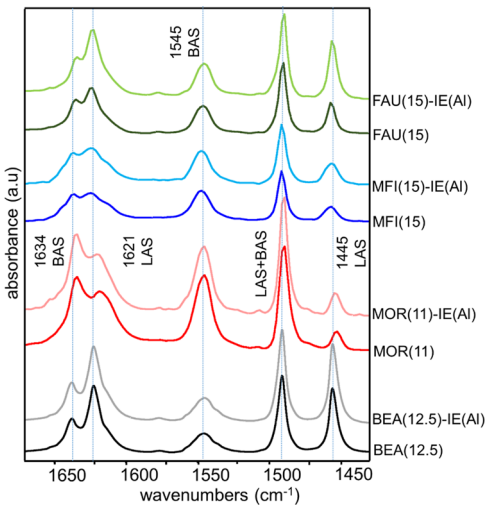

Figure 6. Pyridine-FTIR difference spectra in the pyridine ring deformation region obtained by subtraction of spectra after activation at 723 K from spectra after pyridine adsorption at 423 K followed by evacuation at 423 K.

As presented in Table 4, BEA(12.5) has the maximum concentration of LAS, i.e., 0.17 mmol g^{-1}, whereas the LAS content of MOR(11), MFI(15), and FAU(15) is very low, i.e., in the range of 0.06−0.08 mmol g^{-1}. The concentration of BAS is 0.16, 0.29, 0.20, and 0.18 mmol g^{-1} for BEA(12.5), MOR(11), MFI(15), and FAU(15), respectively, with the maximum being for the MOR(11) zeolite.

After Al-IE, LAS bands do not encounter any significant change in the spectra of MOR(11)-IE(Al) and MFI(15)-IE(Al) compared to those of the respective parent zeolites. Therefore, the LAS content in MOR(11)-IE(Al) and MFI(15)-IE(Al) samples (0.07 and 0.08 mmol g^{-1}, respectively) is also comparable to that of the parent zeolites. Nevertheless, the intensity of the LAS bands increases in the spectra of FAU(15)-IE(Al) and BEA(12.5)-IE(Al), with the spectrum of FAU(15)-IE(Al) showing a maximum increase. Likewise, there is a moderate increase in the LAS content of BEA(12.5)-IE(Al), i.e., 0.20 mmol g^{-1}; however, FAU(15)-IE(Al) shows LAS content of 0.15 mmol g^{-1} which is fairly large as compared to FAU(15). Thus, the LAS content after Al-IE decreases in the following order: BEA(12.5)-IE(Al) > FAU(15)-IE(Al) > MOR(11)-IE(Al) ≈ MFI(15)-IE(Al).

Table 4. LAS and BAS Concentration in mmoles g^{-1} (±10%) Obtained from Pyridine-FTIR Spectroscopy

zeolite	Py-LAS[a]	Py-BAS[a]	conversion[b]	initial rate[c]	*cis*/*trans*[d]
BEA(12.5)	0.17	0.16	96	1.67	94:06
BEA(12.5)-IE(Al)	0.20	0.15	100	1.9	88:12
MOR(11)	0.06	0.29	10	0.03	45:55
MOR(11)-IE(Al)	0.07	0.27	9	0.04	39:61
MFI(15)	0.07	0.20	9	0.04	37:63
MFI(15)-IE(Al)	0.08	0.21	10	0.05	34:66
FAU(15)	0.06	0.18	24	0.08	25:75
FAU(15)-IE(Al)	0.15	0.19	99	0.26	10:90

[a]Catalytic data of MPV reduction of 4-*tert*-butylcyclohexanone (±5%). [b]Conversion of 4-*tert*-butylcyclohexanone over after 7.4 h. [c]Initial rate of reaction in mmoles L^{-1} min^{-1}. [d]Cumulative selectivity after 7.4 h to *cis* and *trans* 4-*tert*-butylcyclohexanol.

https://doi.org/10.1021/acscatal.3c04195
ACS Catal. 2024, 14, 678−690

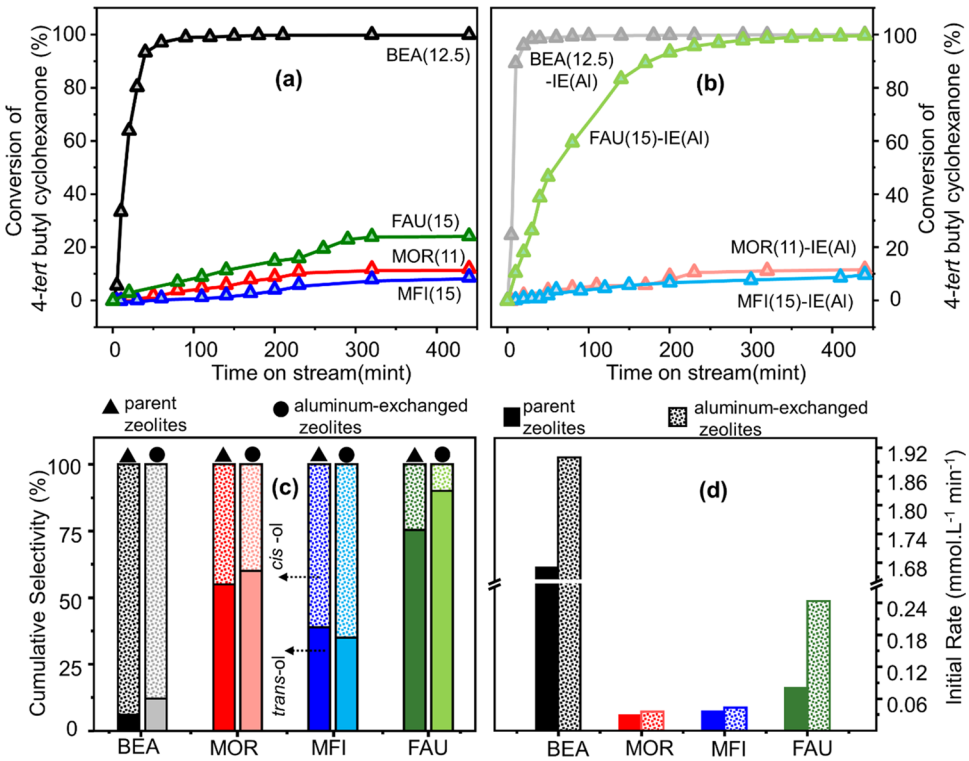

Figure 7. Catalytic conversion (%) of 4-*tert*-butylcyclohexanone as a function of time on stream over parent (a) and aluminum-exchanged (b) zeolites. Cumulative selectivity (c) toward *cis* (dotted bars) and *trans* (solid bars) 4-*tert*-butylcyclohexanol for parent (▲) and aluminum-exchanged zeolites (●). Initial rate of reaction (d) of parent (solid bars) and aluminum-exchanged zeolites (dotted bars), determined as the slope of the linear regression in the time−concentration plot between zero time and 110 min of reaction time.

No prominent increase/decrease in the intensity of bands of BAS arises due to Al-IE in any of the spectra of aluminum-exchanged samples (staying within the error limits of ±10%).[37] As a result, the concentration of BAS after Al-IE is comparable to that of parent zeolites, even for FAU(15)-IE(Al), which shows a maximum increase in Lewis acidity. Furthermore, the number of acid sites quantified by FTIR is an order of magnitude lower than the aluminum species quantified from NMR. Such a difference is common for the IR of any probe molecule, as the amount of acid sites a probe molecule measures depends on the strength of acid sites and pKb of the used base as well as the size of the molecule.

2.3. Lewis Acid Catalytic Activity. The catalytic Meerwein−Ponndorf−Verley reduction of 4-*tert*-butylcyclohexanone, using isopropanol as the reducing agent, was performed to compare the catalytic performance of the parent and aluminum-exchanged zeolites (Figure 7a−d and Table 4). In the case of FAU(15), the reaction rate is 0.08 mmol L^{-1} min^{-1}, and the conversion increased with time on stream, reaching 24%. BEA(12.5) outperforms all parent zeolites, showing a steep increase in conversion within 2 h of reaction time, and reaches the maximum conversion of 96% at a very high initial rate of 1.67 mmol L^{-1} min^{-1} (Figure 7d and Table 4). As *cis* and *trans* 4-*tert*-butylcyclohexanol are the two reaction products, there is a significant difference in the ratio of *cis* to *trans*-ol cumulative selectivity in parent zeolites (Figure 7c and Table 4). It appears that BEA(12.5) is most selective toward *cis*-ol (*cis*/*trans* selectivity of 94:06), whereas FAU(15) exhibits the greatest selectivity to the *trans* product (*cis*/*trans* ratio of 25:75 respectively).

The most prominent variation upon Al-IE in catalytic performance (as compared to parent zeolites) occurred in the case of FAU(15)-IE(Al), where the conversion increases sharply during the time on stream and reaches a very high value of 99%, at a very high reaction rate of 0.26 mmol L^{-1} min^{-1} (Figure 7b,7d and Table 4). The increase in catalytic activity is also followed by a 15% increase in the *trans*-ol selectivity, with the *cis*/*trans* selectivity reaching 10:90% (Figure 7c and Table 4). Similarly, in BEA(12.5)-IE(Al), Al-IE increases the ketone conversion to 100% within the reaction time studied, with a higher rate of reaction of 1.90 mmol L^{-1} min^{-1}, whereas the *cis*/*trans* selectivity remains comparable to that of the parent zeolite (Figure 7d and Table 4). The catalytic data of MOR and MFI zeolites are discussed in detail in the SI (Section S2).

Thus, the catalytic activity of parent zeolites follows the order: BEA(12.5) > FAU(15) > MOR(11) ≈ MFI(15). However, the increase in the catalytic activity of aluminum-exchanged samples, when compared with that of their respective parent zeolites, decreases in the following order: FAU(15)-IE(Al) > BEA(12.5)-IE(Al) > MOR(11)-IE(Al) ≈ MFI(15)-IE(Al). Thus, BEA(12.5)-IE(Al) has the highest catalytic activity among all of the parent and aluminum-exchanged zeolites.

Since parent BEA(12.5) inherits a large concentration of LAS (Table 4), and it already shows 96% conversion, it is rather difficult to observe the potential effect of EFAl LAS incorporated by Al-IE (only 4% increase). Therefore, BEA(150) zeolite with a very low concentration of LAS and comparatively lower conversion (42%) and its respective aluminum-exchanged sample, i.e., BEA(12.5)-IE(Al), were also tested (Table S3). After Al-IE, the conversion reaches 100%, with a significant change in the rate of reaction (0.3 to 1.59

https://doi.org/10.1021/acscatal.3c04195
ACS Catal. 2024, 14, 678−690

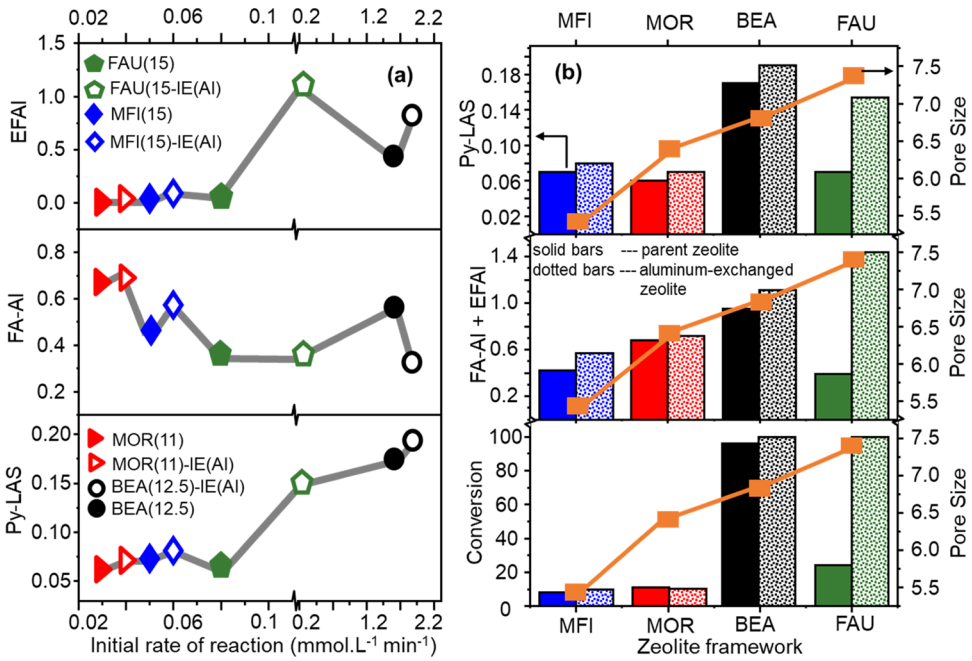

Figure 8. Total LAS content (mmol g^{-1}) determined by Py-FTIR and concentration of FA-Al and EFAl species (mmol g^{-1}) determined by NMR plotted as a function of the initial rate of reaction (a); total MPV conversion (%) after 7.4 h, sum of the concentration of FA-Al and EFAl species (mmol g^{-1}) and total LAS content (mmol g^{-1}) in parent and aluminum-exchanged zeolites (b); orange curves with squares in panel (b) represent the pore size of MFI, BEA, MOR, and FAU zeolites.

mmol L^{-1} min^{-1}), whereas *cis*/*trans* selectivity does not vary much when compared to the BEA(150) sample (Table S3).

2.4. Factors Affecting the Generation and Activity of Extra-Framework Lewis Acid Sites in Different Zeolites. Figure 8a,b comprehensively compare LAS from pyridine FTIR (Py-FTIR) and the concentration of FA-Al and EFAl species as functions of MPV catalytic activity and pore size. Due to postsynthetic modifications, the FA-Al and EFAl species are generated in parent zeolites (Section S3).

The reversibility of FA-Al, from octahedral to tetrahedral coordination, depends on the conditions applied (Figure S4).[20] At higher temperatures, dehydration would cause the loss of excess water hydration, resulting in tetrahedral coordination of these species. However, this may not be the case at lower temperatures, such as those used for MPV reactions (~80 °C). Furthermore, aluminum zeolites are hydrophilic in nature. Therefore, in MPVO-type reactions, the solvation ability of isopropyl alcohol and the water in it would retain the Lewis acidic nature and octahedral coordination of FA-Al. Both FA-Al and EFAl species contribute to Lewis acidity, as the inherent Lewis acidity of FAU(15) and MOR(11) is solely due to FA-Al and that of BEA(12.5) and MFI(15) is due to both FA-Al and EFAl species, respectively (Figure 8a,8b).

Literature suggests that the protonic form of steamed BEA zeolites contains both FA-Al and EFAl species, with the former being in the dominant proportion. Zeolite BEA experiences substantial distortions due to its less stable framework, which initiates, after postsynthetic treatments, the opening of the framework Al−O linkages. This results in a considerable amount of FA-Al species,[23,73] whereas severe steaming treatments of BEA zeolites lead to the preferential formation of EFAl species.[30] The presence of FA-Al LAS in MOR and FAU has also been discussed in recent literature.[13,14,37] Similarly, the presence of resonance due to FA-Al species (~0 ppm) in protonic MFI zeolite resulted in the appearance of Lewis acidic band (~1455 cm^{-1}) in Py-FTIR spectra.[74]

The highest catalytic activity and Lewis acidity of BEA(12.5) among all parent zeolites (Figure 8a,8b) are governed by the framework type, which, in the case of BEA(12.5), is defective and can possess a substantial concentration of Lewis acid sites in the form of defect sites (Section S3). Moreover, the Lewis acidic aluminum species located exclusively in the walls of micropores further account for the high activity of BEA(12.5) in MPV reaction and its higher stereoselectivity toward *cis*-4-*tert*-butylcyclohexanol product (Section S3). Due to these reasons, an appreciable increase of EFAl LAS was possible after Al-IE with an associated increase in catalytic activity. In the case of FAU(15), the concentration of the FA-Al species nicely correlates with the inherent Lewis acid content measured by FTIR of adsorbed pyridine (Figure 8a). The activity of zeolite FAU(15), greater than that of MFI(15) and MOR(11), can be explained by the fact that it has the widest pores openings among all zeolites studied (Section S3). Because the MPV reaction in FAU also takes place within micropores, FAU shows the highest selectivity toward the *trans*-alcohol. The lower activity of FAU(15) as compared to BEA(12.5) can be explained by the presence of a 4 times greater content of octahedral Al(VI_a) and Al(VIb) aluminum species and at least 2 times greater content of LAS. After Al-IE, the largest pore size of FAU(15) facilitates the maximum incorporation and stabilization of Lewis acidic EFAl and the associated maximum increase in the catalytic performance.

The very low Lewis acidity (accessed by pyridine) and the very low activity in MPV reaction in the case of MOR(11), yet with a very high concentration of FA-Al and wide pore openings, is due to the accessibility limitations offered by 8-MR "side pockets" and the position of FA-Al species (Section S3). This indicates that the distribution of aluminum in the MOR framework plays a significant role in the Lewis acidity

https://doi.org/10.1021/acscatal.3c04195
ACS Catal. 2024, 14, 678−690

Table 5. Summary of Factors Affecting the Generation and Activity of Extra-Framework Lewis Acid Sites in Zeolites Studied in This Work

	Lewis acidic Al species	*cis*/*trans* product selectivity	accessibility limitation (pyridine, MPV ketone/alcohol)	steric hindrance for EFAl	Lewis acid activity, pristine zeolite	increase in Lewis acid activity after Al-IE
BEA(12.5)	FA-Al + EFAl	*cis* (small pore size, LAS present in micropores)	X (size + distorted framework)	X	very high	
BEA(12.5)-IE(Al)	FA-Al + EFAl			X		considerable
MOR(11)	FA-Al	*trans* (large pore size)	√ (due to 8 MR)	√	negligible	
MOR(11)-IE(Al)	FA-Al			√		negligible
MFI(15)	FA-Al + EFAl	*cis* (small pore size)	√ (small pore size)	√	negligible	
MFI(15)-IE(Al)	FA-Al + EFAl			√		negligible
FAU(15)	FA-Al	*trans* (large pore size)	X (large pore size)	X	small	
FAU(15)-IE(Al)	FA-Al + FAl			X		very high

and catalytic activity of the aluminum species. The same factors account for the lowest incorporation of EFAl after Al-IE (Section S3). There is also a second possibility that EFAl species could not be formed/stabilized in the side pockets of zeolite due to the FA-Al already sitting there (Section S3). Furthermore, the difference in the number of acid sites quantified from FTIR and the aluminum species quantified from NMR is most prominent in MOR because pyridine cannot probe the acid sites located in the side pockets (Figure 5).

In the case of the MFI(15) zeolite, the low Lewis acidity accessed by pyridine and the low catalytic activity (Figure 8a,8b) can be explained in terms of its small pore size (Section S3). Furthermore, the large size of aluminum precursor and small pore size of zeolite also administrates the ineffectiveness of the Al-IE procedure to introduce EFAl LAS.

Table 5 summarizes the factors that affect the generation of extra-framework Lewis acid sites and their activity in the MPV reaction. The information obtained from this work clearly demonstrates that Al-IE is an efficient method to increase Lewis acidity without affecting a zeolite's porous structure and crystallinity. As most of the EF aluminum Lewis acid sites generated by Al-IE possess octahedral coordination under NMR conditions and do not affect the total BAS content of zeolites (Figure 8a,b), these neutral species may exist in the form of nanosized oxide and/or hydroxide clusters, as suggested in our previous work.[37] However, the catalytic activity of parent zeolites and the efficiency of Al-IE to introduce Lewis acidic moieties depends on different factors that are relevant in different ways, i.e., type of zeolite framework, pore size, accessibility, distribution of aluminum in zeolite framework, size of aluminum precursor, location of Lewis acidic aluminum, transition state stability, and the symmetry of the reactant (Table 5). The relative selectivity toward *cis*/*trans* 4-*tert*-butylcyclohexanol before and after Al-IE is governed by the zeolite pore size and the location of LAS species and not by the nature of Lewis acidic aluminum they have (Table 5).

Another important factor that can facilitate the accommodation of EFAl in zeolites is the presence of defect sites in the parent zeolites, which are usually associated with postsynthetic treatments. The formation of no/very little EFAl LAS in MOR(11) and MFI(15) after Al-IE is in line with the fact that these zeolites are highly crystalline and contain few defect sites. FAU(15) and BEA (12.5) hold large amounts of defect sites as the commercial synthesis protocol of the former is realized by steaming and acid-leaching treatments,[48] whereas that of the latter employs alkalies as mineralizing agents (that cannot form defect-free BEA),[75] respectively. Therefore, the positive effect of the presence of defect sites also holds well for FAU(15) and BEA(12.5). This is further supported by the fact that BEA(150), prepared by post-synthetic treatments and likely to have substantial amounts of defect sites, shows a greater concentration of EFAl after Al-IE compared with BEA(12.5) zeolite. However, MOR(45) and MFI(40) do not show any significant increase in EFAl after Al-IE (Figure S2a,b and Table S3).

It has been previously established that a probe molecule, with size and basicity weaker and smaller, respectively, than pyridine (e.g., CH_3CN or carbon monoxide), can help in understanding the possible accessibility limitations due to the large size and strong basicity of pyridine.[20] In this respect, carbon monoxide (smaller in size and weaker in strength as compared to pyridine) is the most widely used probe molecule, which can access the acid sites differently, based on their strength.[13,14] In our previous paper, however, we have shown that after aluminum exchange of zeolite FAU with a Si/Al ratio of 30, the collective increase in intensity of the two LAS bands was not as significant as in the case of Py-FTIR.[37] The carbon monoxide interacts with Lewis acid sites mostly electrostatically, which justifies the weak strength of interaction, and hence, predominantly strong acid sites are probed. As aluminum exchange produces charge-neutral LAS, carbon monoxide does not probe all of the incorporated EFAl species.[37] Detailed insights into accessibility limitations in zeolites under study can be obtained by comparing the Py-FTIR results with qualitative information from smaller probes such as CH_3CN or carbon monoxide.

3. CONCLUSIONS

The aluminum exchange procedure was employed to compare the generation and activity of Lewis acidity in zeolites with those of BEA, MOR, MFI, and FAU topologies. The results indicate that this procedure efficiently incorporates a significant amount of LAS in BEA and FAU zeolites, as determined by the FTIR of adsorbed pyridine. The incorporated LAS in these zeolites and the framework ones have a quantitative correlation with the aluminum content determined by ICP, the octahedrally coordinated EFAl determined by ^{27}Al MAS NMR, and the catalytic activity for MPV reduction of 4-*tert*-butylcyclohexanone. The LAS in BEA and FAU are not incorporated at the expense of BAS and therefore exist as neutral aluminum oxide/hydroxide nanoclusters. These LAS could not be generated in MFI zeolite due to its small pore size and in MOR zeolite due to accessibility limitations caused by side pockets and potential positions of these EFAl LAS in MOR, respectively. Consequently, no

https://doi.org/10.1021/acscatal.3c04195
ACS Catal. 2024, 14, 678−690

significant change in the content of the EFAl and MPV catalytic activity was observable in these zeolites. The respective selectivity, determined by the pore size of all zeolite catalysts, toward *cis* to *trans* 4-*tert*-butylcyclohexanol does not vary after Al-IE treatments.

■ ASSOCIATED CONTENT

Supporting Information

The Supporting Information is available free of charge at https://pubs.acs.org/doi/10.1021/acscatal.3c04195.

Experimental details on synthesis and characterization of materials and catalytic evaluation, figures showing ^{27}Al MAS NMR spectra of parent zeolites in their respective proton and ammonium forms, physicochemical characterization, FTIR spectra, and catalytic data of aluminum-exchanged samples of MFI(40) and MOR(45), reaction schematic for Meerwein−Ponndorf−Verley reduction, and quantitative distribution of aluminum species obtained from ^{27}Al MAS and MQMAS NMR spectra (PDF)

■ AUTHOR INFORMATION

Corresponding Author

Jeroen A. van Bokhoven − *Institute for Chemical and Bioengineering, Department of Chemistry and Applied Biosciences, ETH Zurich, Zurich 8093, Switzerland; Laboratory for Catalysis and Sustainable Chemistry, Paul Scherrer Institute, Villigen 5232, Switzerland;* orcid.org/0000-0002-4166-2284; Email: jeroen.vanbokhoven@chem.ethz.ch

Authors

Syeda R. Batool − *Institute for Chemical and Bioengineering, Department of Chemistry and Applied Biosciences, ETH Zurich, Zurich 8093, Switzerland;* orcid.org/0000-0003-4885-6548

Vitaly L. Sushkevich − *Laboratory for Catalysis and Sustainable Chemistry, Paul Scherrer Institute, Villigen 5232, Switzerland;* orcid.org/0000-0002-3788-8969

Complete contact information is available at: https://pubs.acs.org/10.1021/acscatal.3c04195

Author Contributions

The manuscript was written through the contributions of all authors. All authors have approved the final version of the manuscript. B.S.R. synthesized the samples, performed the experiments, and prepared the manuscript. V.L.S. provided feedback during the FTIR experiments and manuscript preparation. J.A.v.B. devised the overall idea, supervised the experimental progress, and provided feedback during the preparation of the manuscript.

Notes

The authors declare no competing financial interest.

■ ACKNOWLEDGMENTS

The authors thankfully acknowledge the ETH Zurich Platform for financial support. S.R.B. thanks the assistance of Dr. René Verel for NMR measurements.

■ REFERENCES

(1) Galadima, A.; Muraza, O. Role of zeolite catalysts for benzene removal from gasoline via alkylation: A review. *Microporous Mesoporous Mater.* **2015**, *213*, 169−180.

(2) Saravanamurugan, S.; Paniagua, M.; Melero, J. A.; Riisager, A. Efficient Isomerization of Glucose to Fructose over Zeolites in Consecutive Reactions in Alcohol and Aqueous Media. *J. Am. Chem. Soc.* **2013**, *135* (14), 5246−5249.

(3) Vogt, E. T. C.; Weckhuysen, B. M. Fluid catalytic cracking: recent developments on the grand old lady of zeolite catalysis. *Chem. Soc. Rev.* **2015**, *44* (20), 7342−7370.

(4) Taarning, E.; Osmundsen, C. M.; Yang, X.; Voss, B.; Andersen, S. I.; Christensen, C. H. Zeolite-catalyzed biomass conversion to fuels and chemicals. *Energy Environ. Sci.* **2011**, *4* (3), 793−804.

(5) Kubička, D.; Kubičková, I.; Čejka, J. Application of molecular sieves in transformations of biomass and biomass-derived feedstocks. *Catal. Rev.* **2013**, *55* (1), 1−78.

(6) Luo, H. Y.; Lewis, J. D.; Román-Leshkov, Y. Lewis Acid Zeolites for Biomass Conversion: Perspectives and Challenges on Reactivity, Synthesis, and Stability. *Annu. Rev. Chem. Biomol. Eng.* **2016**, *7* (1), 663−692.

(7) Nesterenko, N. S.; Thibault-Starzyk, F.; Montouillout, V.; Yuschenko, V. V.; Fernandez, C.; Gilson, J. P.; Fajula, F.; Ivanova, I. I. Accessibility of the acid sites in dealuminated small-port mordenites studied by FTIR of co-adsorbed alkylpyridines and CO. *Microporous Mesoporous Mater.* **2004**, *71* (1), 157−166.

(8) Zholobenko, V.; Freitas, C.; Jendrlin, M.; Bazin, P.; Travert, A.; Thibault-Starzyk, F. Probing the acid sites of zeolites with pyridine: Quantitative AGIR measurements of the molar absorption coefficients. *J. Catal.* **2020**, *385*, 52−60.

(9) Haag, W. O.; Lago, R. M.; Weisz, P. B. The active site of acidic aluminosilicate catalysts. *Nature* **1984**, *309* (5969), 589−591.

(10) Kentgens, A. P. M.; Iuga, D.; Kalwei, M.; Koller, H. Direct observation of Brønsted acidic sites in dehydrated zeolite H-ZSM5 using DFS-enhanced 27Al MQMAS NMR spectroscopy. *J. Am. Chem. Soc.* **2001**, *123* (12), 2925−2926.

(11) Kanellopoulos, J.; Unger, A.; Schwieger, W.; Freude, D. Catalytic and multinuclear MAS NMR studies of a thermally treated zeolite ZSM-5. *J. Catal.* **2006**, *237* (2), 416−425.

(12) Haag, W. O.; Lago, R.; Weisz, P. The active site of acidic aluminosilicate catalysts. *Nature* **1984**, *309* (5969), 589−591.

(13) Ravi, M.; Sushkevich, V. L.; van Bokhoven, J. A. Lewis acidity inherent to the framework of zeolite mordenite. *J. Phys. Chem. C* **2019**, *123* (24), 15139−15144.

(14) Ravi, M.; Sushkevich, V. L.; van Bokhoven, J. A. On the location of Lewis acidic aluminum in zeolite mordenite and the role of framework-associated aluminum in mediating the switch between Brønsted and Lewis acidity. *Chem. Sci.* **2021**, *12* (11), 4094−4103.

(15) Woolery, G. L.; Kuehl, G. H.; Timken, H. C.; Chester, A. W.; Vartuli, J. C. On the nature of framework Brønsted and Lewis acid sites in ZSM-5. *Zeolites* **1997**, *19* (4), 288−296.

(16) Phung, T. K.; Busca, G. On the Lewis acidity of protonic zeolites. *Appl. Catal., A* **2015**, *504*, 151−157.

(17) Gil, B.; Zones, S. I.; Hwang, S.-J.; Bejblová, M.; Čejka, J. Acidic Properties of SSZ-33 and SSZ-35 Novel Zeolites: a Complex Infrared and MAS NMR Study. *J. Phys. Chem. C* **2008**, *112* (8), 2997−3007.

(18) Jacobs, P. A.; Beyer, H. K. Evidence for the nature of true Lewis sites in faujasite-type zeolites. *J. Phys. Chem. A* **1979**, *83* (9), 1174−1177.

(19) Lohse, U.; Löffler, E.; Hunger, M.; Stöckner, J.; Patzelová, V. Hydroxyl groups of the non-framework aluminium species in dealuminated Y zeolites. *Zeolites* **1987**, *7* (1), 11−13.

(20) Ravi, M.; Sushkevich, V. L.; van Bokhoven, J. A. Towards a better understanding of Lewis acidic aluminium in zeolites. *Nat. Mater.* **2020**, *19* (10), 1047−1056.

(21) Sommer, J.; Jost, R.; Hachoumy, M. Activation of small alkanes on strong solid acids: mechanistic approaches. *Catal. Today* **1997**, *38* (3), 309−319.

(22) Huang, J.; Jiang, Y.; Marthala, V. R. R.; Thomas, B.; Romanova, E.; Hunger, M. Characterization and Acidic Properties of Aluminum-Exchanged Zeolites X and Y. *J. Phys. Chem. C* **2008**, *112* (10), 3811−3818.
(23) Bourgeat-Lami, E.; Massiani, P.; Di Renzo, F.; Espiau, P.; Fajula, F.; Des Courières, T. Study of the state of aluminium in zeolite-*β*. *Appl. Catal.* **1991**, *72* (1), 139−152.
(24) Wouters, B. H.; Chen, T. H.; Grobet, P. J. Reversible Tetrahedral− Octahedral Framework Aluminum Transformation in Zeolite Y. *J. Am. Chem. Soc.* **1998**, *120* (44), 11419−11425.
(25) Haouas, M.; Kogelbauer, A.; Prins, R. The effect of flexible lattice aluminium in zeolite beta during the nitration of toluene with nitric acid and acetic anhydride. *Catal. Lett.* **2000**, *70* (1−2), 61−65.
(26) Omegna, A.; van Bokhoven, J. A.; Prins, R. Flexible Aluminum Coordination in Alumino−Silicates. Structure of Zeolite H-USY and Amorphous Silica−Alumina. *J. Phys. Chem. B* **2003**, *107* (34), 8854−8860.
(27) Ward, J. W. The nature of active sites on zeolites: I. The decationated Y zeolite. *J. Catal.* **1967**, *9* (3), 225−236.
(28) Brus, J.; Kobera, L.; Schoefberger, W.; Urbanová, M.; Klein, P.; Sazama, P.; Tabor, E.; Sklenak, S.; Fishchuk, A. V.; Dědeček, J. Structure of framework aluminum Lewis sites and perturbed aluminum atoms in zeolites as determined by 27Al {1H} REDOR (3Q) MAS NMR spectroscopy and DFT/molecular mechanics. *Angew. Chem., Int. Ed.* **2015**, *54* (2), 541−545.
(29) Catana, G.; Baetens, D.; Mommaerts, T.; Schoonheydt, R. A.; Weckhuysen, B. M. Relating structure and chemical composition with lewis acidity in zeolites: A spectroscopic study with probe molecules. *J. Phys. Chem. B* **2001**, *105* (21), 4904−4911.
(30) Kunkeler, P.; Zuurdeeg, B.; Van Der Waal, J.; van Bokhoven, J. A.; Koningsberger, D.; Van Bekkum, H. Zeolite beta: the relationship between calcination procedure, aluminum configuration, and Lewis acidity. *J. Catal.* **1998**, *180* (2), 234−244.
(31) Lanzafame, P.; Temi, D. M.; Perathoner, S.; Spadaro, A. N.; Centi, G. Direct conversion of cellulose to glucose and valuable intermediates in mild reaction conditions over solid acid catalysts. *Catal. Today* **2012**, *179* (1), 178−184.
(32) Ramli, N. A. S.; Amin, N. A. S. Kinetic study of glucose conversion to levulinic acid over Fe/HY zeolite catalyst. *Chem. Eng. J.* **2016**, *283*, 150−159.
(33) Boronat, M.; Corma, A.; Renz, M.; Viruela, P. M. Predicting the activity of single isolated Lewis acid sites in solid catalysts. *Chem. - Eur. J.* **2006**, *12* (27), 7067−7077.
(34) Konwar, L. J.; Mäki-Arvela, P.; Begum, P.; Kumar, N.; Thakur, A. J.; Mikkola, J.-P.; Deka, R. C.; Deka, D. Shape selectivity and acidity effects in glycerol acetylation with acetic anhydride: Selective synthesis of triacetin over Y-zeolite and sulfonated mesoporous carbons. *J. Catal.* **2015**, *329*, 237−247.
(35) Luo, H. Y.; Consoli, D. F.; Gunther, W. R.; Román-Leshkov, Y. Investigation of the reaction kinetics of isolated Lewis acid sites in Beta zeolites for the Meerwein−Ponndorf−Verley reduction of methyl levulinate to *γ*-valerolactone. *J. Catal.* **2014**, *320*, 198−207.
(36) Corma, A.; Domine, M. E.; Valencia, S. Water-resistant solid Lewis acid catalysts: Meerwein−Ponndorf−Verley and Oppenauer reactions catalyzed by tin-beta zeolite. *J. Catal.* **2003**, *215* (2), 294−304.
(37) Batool, S. R.; Sushkevich, V. L.; van Bokhoven, J. A. Correlating Lewis acid activity to extra-framework aluminum species in zeolite Y introduced by Ion-exchange. *J. Catal.* **2022**, *408*, 24−35.
(38) Almutairi, S. M. T.; Mezari, B.; Filonenko, G. A.; Magusin, P. C.; Rigutto, M. S.; Pidko, E. A.; Hensen, E. J. Influence of extraframework aluminum on the brønsted acidity and catalytic reactivity of faujasite zeolite. *ChemCatChem* **2013**, *5* (2), 452−466.
(39) Al-Nayili, A.; Albdiry, M.; Salman, N. Dealumination of Zeolite Frameworks and Lewis Acid Catalyst Activation for Transfer Hydrogenation. *Arabian J. Sci. Eng.* **2021**, *46* (6), 5709−5716.
(40) Creyghton, E.; Ganeshie, S.; Downing, R.; Van Bekkum, H. Stereoselective Meerwein−Ponndorf−Verley and Oppenauer reactions catalysed by zeolite BEA. *J. Mol. Catal. A: Chem.* **1997**, *115* (3), 457−472.
(41) Jansen, J. C.; Creyghton, E. J.; Njo, S. L.; van Koningsveld, H.; van Bekkum, H. On the remarkable behaviour of zeolite Beta in acid catalysis. *Catal. Today* **1997**, *38* (2), 205−212.
(42) López-Aguado, C.; Paniagua, M.; Iglesias, J.; Morales, G.; García-Fierro, J. L.; Melero, J. A. Zr-USY zeolite: Efficient catalyst for the transformation of xylose into bio-products. *Catal. Today* **2018**, *304*, 80−88.
(43) Paulino, P. N.; Perez, R. F.; Figueiredo, N. G.; Fraga, M. A. Tandem dehydration−transfer hydrogenation reactions of xylose to furfuryl alcohol over zeolite catalysts. *Green Chem.* **2017**, *19* (16), 3759−3763.
(44) International Zeolite Association (IZA). Database of Zeolite Structures, 2023. http://www.iza-structure.org/databases/.
(45) Li, P.; Liu, G.; Wu, H.; Liu, Y.; Jiang, J.-g.; Wu, P. Postsynthesis and Selective Oxidation Properties of Nanosized Sn-Beta Zeolite. *J. Phys. Chem. C* **2011**, *115* (9), 3663−3670.
(46) Lin, J.-S.; Wang, J.-J.; Wang, J.; Wang, I.; Balasamy, R. J.; Aitani, A.; Al-Khattaf, S.; Tsai, T.-C. Catalysis of alkaline-modified mordenite for benzene alkylation of diolefin-containing dodecene for linear alkylbenzene synthesis. *J. Catal.* **2013**, *300*, 81−90.
(47) Li, J.; Liu, H.; An, T.; Yue, Y.; Bao, X. Carboxylic acids to butyl esters over dealuminated−realuminated beta zeolites for removing organic acids from bio-oils. *RSC Adv.* **2017**, *7* (54), 33714−33725.
(48) Zhang, R.; Xu, S.; Raja, D.; Khusni, N. B.; Liu, J.; Zhang, J.; Abdulridha, S.; Xiang, H.; Jiang, S.; Guan, Y.; Jiao, Y.; Fan, X. On the effect of mesoporosity of FAU Y zeolites in the liquid-phase catalysis. *Microporous Mesoporous Mater.* **2019**, *278*, 297−306.
(49) McGlone, J.; Priecel, P.; Da Vià, L.; Majdal, L.; Lopez-Sanchez, J. A. Desilicated ZSM-5 zeolites for the production of renewable p-xylene via Diels−Alder cycloaddition of dimethylfuran and ethylene. *Catalysts* **2018**, *8* (6), 253.
(50) Gackowski, M.; Podobinski, J.; Broclawik, E.; Datka, J. IR and NMR Studies of the Status of Al and Acid Sites in Desilicated Zeolite Y. *Molecules* **2020**, *25* (1), 31.
(51) van Bokhoven, J. A.; Koningsberger, D.; Kunkeler, P.; Van Bekkum, H.; Kentgens, A. Stepwise dealumination of zeolite *β*eta at specific T-sites observed with 27Al MAS and 27Al MQ MAS NMR. *J. Am. Chem. Soc.* **2000**, *122* (51), 12842−12847.
(52) Ray, G. J.; Samoson, A. Double rotation and variable field 27Al n.m.r. study of dealuminated Y zeolites. *Zeolites* **1993**, *13* (6), 410−413.
(53) Kosslick, H.; Tuan, V. A.; Fricke, R.; Martin, A.; Storek, W. Study on the Nature of Aluminum in Dealuminated Zeolite ZSM-20. In *Studies in Surface Science and Catalysis*; Weitkamp, J.; Karge, H. G.; Pfeifer, H.; Hölderich, W., Eds.; Elsevier, 1994; Vol. *84*, pp 1013−1020.
(54) Remy, M. J.; Stanica, D.; Poncelet, G.; Feijen, E. J. P.; Grobet, P. J.; Martens, J. A.; Jacobs, P. A. Dealuminated H−Y Zeolites: Relation between Physicochemical Properties and Catalytic Activity in Heptane and Decane Isomerization. *J. Phys. Chem. A* **1996**, *100* (30), 12440−12447.
(55) Czjzek, G.; Fink, J.; Götz, F.; Schmidt, H.; Coey, J.; Rebouillat, J.-P.; Liénard, A. Atomic coordination and the distribution of electric field gradients in amorphous solids. *Phys. Rev. B* **1981**, *23* (6), 2513.
(56) Zecchina, A.; Bordiga, S.; Spoto, G.; Marchese, L.; Petrini, G.; Leofanti, G.; Padovan, M. Silicalite characterization. 2. IR spectroscopy of the interaction of carbon monoxide with internal and external hydroxyl groups. *J. Phys. Chem. A* **1992**, *96* (12), 4991−4997.
(57) Wu, P.; Komatsu, T.; Yashima, T. IR and MAS NMR studies on the incorporation of aluminum atoms into defect sites of dealuminated mordenites. *J. Phys. Chem. A* **1995**, *99* (27), 10923−10931.
(58) Nogier, J.-P.; Millot, Y.; Man, P. P.; Shishido, T.; Che, M.; Dzwigaj, S. Probing the Incorporation of Ti(IV) into the BEA Zeolite Framework by XRD, FTIR, NMR, and DR UV−jp810722bis. *J. Phys. Chem. C* **2009**, *113* (12), 4885−4889.

(59) Holm, M. S.; Svelle, S.; Joensen, F.; Beato, P.; Christensen, C. H.; Bordiga, S.; Bjørgen, M. Assessing the acid properties of desilicated ZSM-5 by FTIR using CO and 2,4,6-trimethylpyridine (collidine) as molecular probes. *Appl. Catal., A* **2009**, *356* (1), 23−30.
(60) Daniell, W.; Topsøe, N.-Y.; Knözinger, H. An FTIR study of the surface acidity of USY zeolites: Comparison of CO, CD3CN, and C5H5N probe molecules. *Langmuir* **2001**, *17* (20), 6233−6239.
(61) Hadjiivanov, K. Identification and Characterization of Surface Hydroxyl Groups by Infrared Spectroscopy. In *Advances in Catalysis*; Elsevier, 2014; Vol. *57*, pp 99−318.
(62) Zecchina, A.; Bordiga, S.; Spoto, G.; et al. Low-temperature Fourier-transform infrared investigation of the interaction of CO with nanosized ZSM5 and silicalite. *J. Chem. Soc., Faraday Trans.* **1992**, *88* (19), 2959−2969.
(63) Kiricsi, I.; Flego, C.; Pazzuconi, G.; Parker, W. O., Jr.; Millini, R.; Perego, C.; Bellussi, G. Progress toward Understanding Zeolite.beta. Acidity: An IR and 27Al NMR Spectroscopic Study. *J. Phys. Chem. A* **1994**, *98* (17), 4627−4634.
(64) Vimont, A.; Thibault-Starzyk, F.; Lavalley, J. Infrared spectroscopic study of the acidobasic properties of beta zeolite. *J. Phys. Chem. B* **2000**, *104* (2), 286−291.
(65) Gould, N. S.; Xu, B. Quantification of acid site densities on zeolites in the presence of solvents via determination of extinction coefficients of adsorbed pyridine. *J. Catal.* **2018**, *358*, 80−88.
(66) Emeis, C. A. Determination of Integrated Molar Extinction Coefficients for Infrared Absorption Bands of Pyridine Adsorbed on Solid Acid Catalysts. *J. Catal.* **1993**, *141* (2), 347−354.
(67) Wang, Y.; Yokoi, T.; Namba, S.; Tatsumi, T. Effects of dealumination and desilication of beta zeolite on catalytic performance in n-hexane cracking. *Catalysts* **2016**, *6* (1), 8.
(68) Dzwigaj, S.; Millot, Y.; Krafft, J.-M.; Popovych, N.; Kyriienko, P. Incorporation of silver atoms into the vacant T-atom sites of the framework of SiBEA zeolite as mononuclear Ag (I) evidenced by XRD, FTIR, NMR, DR UV−vis, XPS, and TPR. *J. Phys. Chem. C* **2013**, *117* (24), 12552−12559.
(69) Coelho, T. L.; Marinho, B.; Albuquerque, E. M.; Fraga, M. A. Discussing the performance of beta zeolites in aqueous-phase valorization of xylose. *Catal. Sci. Technol.* **2020**, *10* (21), 7165−7176.
(70) Deng, J.; Liu, J.; Song, W.; Zhao, Z.; Zhao, L.; Zheng, H.; Lee, A. C.; Chen, Y.; Liu, J. Selective catalytic reduction of NO with NH 3 over Mo−Fe/beta catalysts: the effect of Mo loading amounts. *RSC Adv.* **2017**, *7* (12), 7130−7139.
(71) Vlasenko, N. V.; Kochkin, Y. N.; Telbiz, G. M.; Shvets, O. V.; Strizhak, P. E. Insight into the active site nature of zeolite H-BEA for liquid phase etherification of isobutylene with ethanol. *RSC Adv.* **2019**, *9* (62), 35957−35968.
(72) Maache, M.; Janin, A.; Lavalley, J.; Joly, J.; Benazzi, E. Acidity of zeolites Beta dealuminated by acid leaching: An FTIR study using different probe molecules (pyridine, carbon monoxide). *Zeolites* **1993**, *13* (6), 419−426.
(73) Kiricsi, I.; Flego, C.; Pazzuconi, G.; Parker, W. J.; Millini, R.; Perego, C.; Bellussi, G. Progress toward understanding zeolite. beta. acidity: an IR and 27Al NMR spectroscopic study. *J. Phys. Chem. A* **1994**, *98* (17), 4627−4634.
(74) Sanhoob, M. A.; Shafei, E. N.; Khan, A.; Nasser, G. A.; Bakare, I.; Muraza, O.; Al-Bahar, M. Z.; Al-Jishi, A. N.; Al-Badairy, H. H.; Ummer, A. C. Catalytic Cracking of n-Dodecane to Chemicals: Effect of Variable-Morphological ZSM-5 Zeolites Synthesized Using Various Silica Sources. *ACS Omega* **2022**, *7* (12), 10317−10329.
(75) Cannan, T.; Hinchey, R. Synthesis of Zeolite Beta. U.S. Patent US5139759A1992.

https://doi.org/10.1021/acscatal.3c04195
ACS Catal. 2024, 14, 678−690